Dynamic regulation of FGF23 by Fam20C phosphorylation, GalNAc-T3 glycosylation, and furin proteolysis

Vincent S. Tagliabracci[a], James L. Engel[a,1], Sandra E. Wiley[a], Junyu Xiao[a], David J. Gonzalez[a,b], Hitesh Nidumanda Appaiah[c], Antonius Koller[d], Victor Nizet[b,e], Kenneth E. White[c], and Jack E. Dixon[a,f,g,2]

Departments of [a]Pharmacology, [b]Pediatrics, [f]Cellular and Molecular Medicine, and [g]Chemistry and Biochemistry and [e]Skaggs School of Pharmacy and Pharmaceutical Sciences, University of California, San Diego, La Jolla, CA 92093; [c]Department of Medical and Molecular Genetics, Indiana University School of Medicine, Indianapolis, IN 46202; and [d]Stony Brook University Proteomics Center, School of Medicine, Stony Brook University, Stony Brook, NY 11794

Contributed by Jack E. Dixon, February 8, 2014 (sent for review January 23, 2014)

The family with sequence similarity 20, member C (Fam20C) has recently been identified as the Golgi casein kinase. Fam20C phosphorylates secreted proteins on Ser-x-Glu/pSer motifs and loss-of-function mutations in the kinase cause Raine syndrome, an often-fatal osteosclerotic bone dysplasia. Fam20C is potentially an upstream regulator of the phosphate-regulating hormone fibroblast growth factor 23 (FGF23), because humans with *FAM20C* mutations and *Fam20C* KO mice develop hypophosphatemia due to an increase in full-length, biologically active FGF23. However, the mechanism by which Fam20C regulates FGF23 is unknown. Here we show that Fam20C directly phosphorylates FGF23 on Ser^{180}, within the FGF23 R^{176}XXR^{179}/S^{180}AE subtilisin-like proprotein convertase motif. This phosphorylation event inhibits O-glycosylation of FGF23 by polypeptide *N*-acetylgalactosaminyltransferase 3 (GalNAc-T3), and promotes FGF23 cleavage and inactivation by the subtilisin-like proprotein convertase furin. Collectively, our results provide a molecular mechanism by which FGF23 is dynamically regulated by phosphorylation, glycosylation, and proteolysis. Furthermore, our findings suggest that cross-talk between phosphorylation and O-glycosylation of proteins in the secretory pathway may be an important mechanism by which secreted proteins are regulated.

phosphate homeostasis | rickets | Fam20 | familial tumoral calcinosis | chronic kidney disease

Protein kinases are evolutionarily conserved enzymes that regulate numerous cellular processes by transferring a molecule of phosphate from ATP to target substrates (1, 2). The vast majority of theses enzymes function within the nucleus and cytosol. In contrast, there are several examples of phosphorylated proteins that are secreted from the cell, which raises the question: What are the kinases that phosphorylate these secreted phosphoproteins? We recently identified a small family of secretory pathway kinases that phosphorylate secreted proteins and proteoglycans (3). These enzymes have N-terminal signal sequences that direct them to the lumen of the endoplasmic reticulum, where they encounter the proteins or proteoglycans that they phosphorylate. One member of this atypical kinase family is the family with sequence similarity 20, member C (Fam20C), which phosphorylates secreted proteins on Ser(S)-x-Glu(E)/pSer(pS) (S-x-E/pS) motifs (3, 4). Because Fam20C localizes within the secretory pathway and the vast majority of secreted phosphoproteins are phosphorylated on S-x-E/pS motifs, Fam20C has been proposed to play a major role in the generation of the secreted phosphoproteome (5–7). For example, ∼75% of human serum and cerebrospinal fluid phosphoproteins are phosphorylated on S-x-E/pS motifs (8, 9). This includes proteins important for tooth and bone formation, as well as numerous hormones. In most cases, the functional importance of these phosphorylation events is unknown.

Loss-of-function mutations in the human *FAM20C* gene cause Raine syndrome, an often-fatal osteosclerotic bone dysplasia (10, 11). Most Raine patients die within the first few weeks of life. Nonlethal cases have also been reported, and these patients develop hypophosphatemia as a result of elevated levels of the phosphate-regulating hormone fibroblast growth factor 23 (FGF23) (12). Additionally, *Fam20C* knockout (KO) mice develop renal phosphate wasting due to an increase in circulating bioactive FGF23 as well as severe hypophosphatemic rickets (13, 14). Thus, Fam20C has been proposed to be a regulator of FGF23; however, the molecular mechanisms underlying the control of this hormone by Fam20C are unclear.

FGF23 is secreted from osteoblasts and osteocytes, and targets the kidney to regulate the reabsorption of phosphate and catabolism of 1,25-dihydroxyvitamin D_3 (15, 16). FGF23 inhibits renal phosphate transport by activating FGF receptors (FGFRs) in a manner that requires binding the coreceptor α-klotho (α-KL) (17). Binding of FGF23 to FGFRs/α-KL induces urinary excretion of phosphate by decreasing the abundance of the type II sodium-dependent phosphate cotransporters NPT2a and NPT2c (15, 16). Several genetic disorders of renal phosphate wasting are associated with alterations in FGF23 (18). X-linked hypophosphatemia is the most prevalent form of hypophosphatemic rickets (1:20,000), and is caused by loss-of-function mutations in the gene encoding the phosphate-regulating endopeptidase homolog X-linked, which is associated with elevated FGF23 expression (19, 20). A similar situation exists in patients with an autosomal recessive form of hypophosphatemic rickets caused by mutations in the ectonucleotide pyrophosphatase ENPP1 (21) and the Fam20C substrate dentin

Significance

The family with sequence similarity 20, member C (Fam20C) is a secretory pathway-specific kinase that phosphorylates secreted proteins on Ser-x-Glu/pSer motifs. Mutations in human *FAM20C* cause a devastating childhood disorder known as Raine syndrome. Some patients with *FAM20C* mutations as well as *Fam20C* KO mice develop hypophosphatemia due to elevated levels of the phosphate-regulating hormone FGF23. In this paper, we show that Fam20C phosphorylates FGF23 on a Ser-x-Glu motif that lies within a critical region of the hormone. The phosphorylation promotes FGF23 proteolysis by furin by blocking O-glycosylation by polypeptide *N*-acetylgalactosaminyltransferase 3. Our results have important implications for patients with abnormalities in phosphate homeostasis.

Author contributions: V.S.T., J.L.E., S.E.W., J.X., and J.E.D. designed research; V.S.T., J.L.E., S.E.W., J.X., D.J.G., and A.K. performed research; H.N.A., A.K., V.N., and K.E.W. contributed new reagents/analytic tools; V.S.T., J.L.E., S.E.W., J.X., D.J.G., H.N.A., A.K., V.N., K.E.W., and J.E.D. analyzed data; and V.S.T., K.E.W., and J.E.D. wrote the paper.

The authors declare no conflict of interest.

Freely available online through the PNAS open access option.

[1]Present address: Molecular, Cellular & Integrative Physiology Graduate Program, Department of Medicine, University of California, Los Angeles, CA 90095.

[2]To whom correspondence should be addressed. E-mail: jedixon@ucsd.edu.

This article contains supporting information online at www.pnas.org/lookup/suppl/doi:10.1073/pnas.1402218111/-/DCSupplemental.

matrix protein 1 (DMP1) (22). These disorders share the common denominator of elevated FGF23.

Other Mendelian disorders of renal phosphate handling have provided important insight into the regulation of FGF23 protein processing. FGF23 is inactivated in the Golgi by proteolysis within a highly conserved subtilisin-like proprotein convertase (SPC) site, ^{176}RHTR^{179}/S^{180}AE^{182}, generating inactive N- and C-terminal fragments (23). Gain-of-function missense mutations in FGF23 cause autosomal dominant hypophosphatemic rickets (ADHR) (24). These mutations substitute the Arg (R) residues within the SPC cleavage site and render the protein resistant to proteolysis (25). Conversely, loss-of-function mutations in FGF23 cause familial tumoral calcinosis (FTC), a hyperphosphatemic disorder characterized by often severe ectopic and vascular calcifications (26). FTC is also caused by loss-of-function mutations in polypeptide *N*-acetylgalactosaminyltransferase 3 (GalNAc-T3), a glycosyltransferase that O-glycosylates FGF23 at Thr^{178} within the SPC cleavage site (27, 28). These inactivating GalNAc-T3 mutations prevent O-glycosylation of FGF23, which produces a hormone more susceptible to SPC proteolysis (28, 29). Collectively, these studies suggest that FGF23 processing is a highly regulated and physiologically important process.

Here we demonstrate that Fam20C regulates FGF23 by phosphorylation of Ser^{180}, a residue that neighbors the SPC site (R^{176}H^{177}T^{178}R^{179}/S^{180}). We show that Ser^{180} phosphorylation inhibits GalNAc-T3 O-glycosylation of Thr^{178}, thereby promoting furin (PCSK3)-dependent FGF23 proteolysis. Our results provide a plausible molecular mechanism by which loss of Fam20C leads to elevated levels of intact, biologically active FGF23 and subsequent hypophosphatemia. Furthermore, our results suggest that cross-talk between phosphorylation and O-glycosylation of proteins in the secretory pathway may be an important mechanism by which secreted proteins are dynamically regulated.

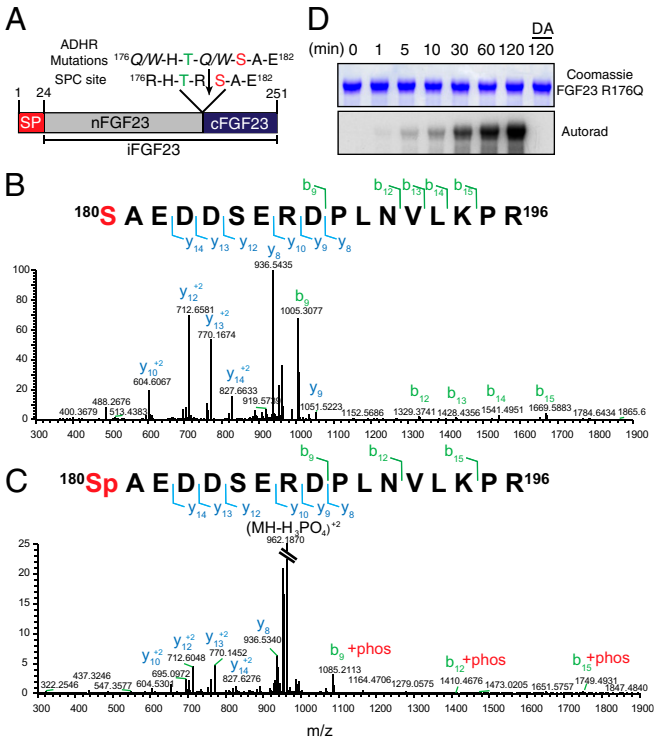

Fig. 1. Fam20C phosphorylates FGF23 on Ser^{180}. (*A*) Schematic representation of human FGF23 indicating the signal peptide (SP), intact FGF23 (iFGF23), N-terminal fragment (nFGF23), and C-terminal fragment (cFGF23). The residues surrounding the SPC cleavage site (downward arrow) are shown. Mutations that replace the Arg in patients with autosomal dominant hypophosphatemic rickets (ADHR) are also shown. A potential Fam20C phosphorylation site is in red. (*B* and *C*) Representative MS/MS fragmentation spectra of a tryptic peptide (FGF23 180–196) depicting Ser^{180} phosphorylation of FGF23 R176Q purified from conditioned medium of HEK293T cells. (*D*) Time-dependent incorporation of ^{32}P from [γ-^{32}P]ATP into FGF23 R176Q by Fam20C or Fam20C D478A (DA). Reaction products were analyzed by SDS/PAGE and autoradiography.

Results

FGF23 Is Phosphorylated by Fam20C in Vitro and in Cells. Contemporaneous with our finding that Fam20C is a protein kinase, Wang et al. (13) characterized *Fam20C* KO mice and demonstrated that these animals develop hypophosphatemic rickets as a result of elevated serum intact, bioactive FGF23. Furthermore, a recent report identified compound heterozygous mutations in *FAM20C* in two siblings referred for hypophosphatemia and severe dental demineralization disease (12). Biochemical analysis of the patients' sera identified elevated intact FGF23. Because FGF23 is expressed in tissues that show high levels of Fam20C expression (30) and contains Fam20C consensus S-x-E/pS motifs (Fig. 1*A*), we hypothesized that Fam20C may directly regulate FGF23 by phosphorylation. To determine whether FGF23 is a phosphoprotein, we generated a HEK293T cell line stably expressing a protease-resistant mutant of FGF23 (FGF23 R176Q) (25). This construct contained a C-terminal Flag tag that allowed us to affinity-purify it from conditioned medium. We then digested FGF23 R176Q with trypsin or chymotrypsin, separated the peptides by liquid chromatography, and analyzed the peptides by mass spectrometry (MS). Tandem mass spectrometry (MS/MS) analysis identified ^{180}pSAEDDSERDPLNVLKPR^{196} and ^{178}TRpSAEDDSERDPL^{190} in the trypsin and chymotrypsin digests, respectively (Fig. 1 *B* and *C* and Fig. S1). These results suggest that FGF23 is phosphorylated in HEK293T cells on Ser^{180}. Notably, Ser^{180} lies within a Fam20C S-x-E recognition motif and neighbors the SPC recognition site (Fig. 1*A*). To test whether Fam20C phosphorylates FGF23, we performed in vitro kinase reactions with recombinant Fam20C and FGF23 R176Q. Fam20C phosphorylated FGF23 R176Q in a time-dependent manner, whereas the catalytically inactive Fam20C D478A failed to incorporate phosphate (Fig. 1*D*). Furthermore, treatment of purified FGF23 R176Q with recombinant Fam20C increased the relative abundance of Ser^{180} phosphorylation (Fig. S2). By calculating the area under the selected ion species, we estimated that treatment with Fam20C increased the relative abundance of FGF23 R176Q Ser^{180} phosphorylation ∼10-fold.

To determine whether Fam20C phosphorylates FGF23 in cells, we used clustered regularly interspaced short palindromic repeats (CRISPR/Cas9) genome-editing technology to delete the *FAM20C* gene from the osteoblast-like cell line U2OS (31, 32) (Fig. S3*A*). We generated U6-driven expression cassettes to express single-guide RNAs targeting exon 1 of the human *FAM20C* gene for expression in U2OS cells (Fig. S3 *B* and *D*). Two clones were detected to have insertions/deletions (indels) that resulted in frameshift mutations resulting in premature stop codons (Fig. S3 *C* and *E*). Protein immunoblotting with a polyclonal antibody raised against full-length Fam20C detected Fam20C protein in the conditioned medium of native U2OS cells but not the cells that were subjected to genome editing (Fig. 2*A*). To confirm loss of Fam20C activity, the phosphorylation status of the Fam20C substrate osteopontin (OPN) was analyzed in control and Fam20C KO cells that were metabolically labeled with [^{32}P]orthophosphate. V5-tagged OPN was immunoprecipitated from conditioned medium, and OPN protein and phosphorylation levels were analyzed by autoradiography. OPN was phosphorylated in control cells, and no detectable phosphorylation was observed in Fam20C KO cells (Fig. 2*B*).

In U2OS cells, ectopically expressed, C-terminal V5-tagged FGF23 is O-glycosylated, and we can detect the full-length hormone and the C-terminal fragments in the conditioned medium by protein immunoblotting of V5-immunoprecipitates (Fig. 2*C*). We transiently transfected V5-tagged FGF23 in control and Fam20C KO cells that we metabolically labeled with [^{32}P]orthophosphate and analyzed V5-immunoprecipitates from

conditioned medium. FGF23 was phosphorylated in control but not in Fam20C-deficient cells, and phosphorylation was more prevalent within the C-terminal fragment (Fig. 2*D*). Thus, Fam20C phosphorylates FGF23 in vitro and in cells.

Phosphorylation of FGF23 at Ser^{180} Prevents O-Glycosylation by GalNAc-T3. The physiological significance of FGF23 O-glycosylation was underscored when inactivating mutations in the gene encoding GalNAc-T3 (*GALNT3*) were found in patients with FTC (27). Patients with FTC develop hyperphosphatemia and severe ectopic calcifications, symptoms of which are the metabolic "mirror image" of the hypophosphatemic disorders (26). Subsequent studies identified inactivating mutations in FGF23 in FTC patients without mutations in *GALNT3*, suggesting that FGF23 and GalNAc-T3 operate in a common pathway to regulate phosphate homeostasis (26). The polypeptide *N*-acetylgalactosaminyltransferase (GalNAc-transferase) family consists of 20 enzymes that catalyze the initial step of mucin-type O-glycosylation by transferring GalNAc from UDP-GalNAc to Ser and Thr residues in secretory pathway proteins (33). GalNAc-T3 O-glycosylates FGF23 on Thr^{178} within the R^{176}H^{177}T^{178}R^{179}/S^{180} SPC site, and has been shown to protect FGF23 from proteolytic cleavage and thus inactivation (28). Because Fam20C phosphorylates FGF23 at Ser^{180}, and this residue is located immediately adjacent to the SPC site (Fig. 1*A*), we hypothesized that phosphorylation may regulate FGF23 O-glycosylation and/or proteolytic processing. In Fam20C-deficient U2OS cells, we did not observe changes in O-glycosylation or proteolytic processing of ectopically expressed FGF23. However, it is likely that endogenous Fam20C levels and/or activity are much lower than the glycosyltransferases and/or proteases that modify FGF23 in these cells (i.e., Fam20C is limiting with respect to the glycosyltransferases and/or proteases). Deletion of Fam20C therefore would have no effect on O-glycosylation and/or processing. To explore the effect of phosphorylation of FGF23 on O-glycosylation and proteolytic processing, we coexpressed Flag-tagged Fam20C or the catalytically inactive Fam20C D478A mutant with V5-tagged FGF23 in U2OS cells and analyzed immunoprecipitates from conditioned medium. Wild-type Fam20C, but not the inactive D478A mutant, decreased the mobility of the C-terminal fragments of FGF23 that was reversed by λ-phosphatase treatment, suggesting a phosphorylation event (Fig. 3*A*, *Lower*, first, second, and third lanes). Interestingly, the doublet in full-length, intact FGF23 (iFGF23) was absent when active Fam20C, but not the inactive Fam20C D478A mutant, was expressed (Fig. 3*A*, *Upper*, first and second lanes). Given the close proximity of Ser^{180} to the SPC site, we reasoned that phosphorylation of FGF23 at Ser^{180} would prevent O-glycosylation at Thr^{178} and therefore explain the loss of the doublet observed in iFGF23 induced by Fam20C (Fig. 3*A*, second lane). Indeed, mutation of Ser^{180} to Ala prevented the loss of the doublet in iFGF23 when Fam20C was expressed (Fig. 3*A*, fourth lane). Consistently, mutation of Thr^{178} to Ala (a nonglycosylated mutant) or Ser^{180} to Asp (a phosphomimetic) resulted in a species that migrated similar to the phosphorylated WT iFGF23 (Fig. 3*A*, fifth and sixth lanes). These results support that Fam20C phosphorylation of FGF23 at Ser^{180} prevents O-glycosylation at Thr^{178}.

To determine whether phosphorylation of FGF23 Ser^{180} directly affects O-glycosylation of FGF23 at Thr^{178} by GalNAc-T3, we produced a HEK293T cell line stably expressing a secreted form of GalNAc-T3 lacking the first 37 residues encompassing the transmembrane domain and immunopurified the enzyme from conditioned medium (sGalNAc-T3; residues 38–633; Fig. S4). We then performed in vitro glycosylation experiments with sGalNAc-T3 and a peptide substrate surrounding the SPC cleavage site of FGF23 [residues 172–190 of human FGF23; hereafter referred to as FGF23(172–190)]. MALDI-TOF MS analysis of the reaction products demonstrated that sGalNAc-T3 catalyzed the transfer of GalNAc from UDP-GalNAc to Thr^{178} of FGF23(172–190) as expected (Fig. 3*B* and Figs. S5*A* and S6). However, when sGalNAc-T3 was assayed against Ser^{180}-phosphorylated FGF23(172–190), no detectable glycosylation was observed upon extended incubation (Fig. 3*C* and Fig. S5*B*). Collectively, our data support that Fam20C phosphorylates FGF23 at Ser^{180} and inhibits O-glycosylation by GalNAc-T3 at Thr^{178}. Importantly, these results provide a molecular mechanism that could account for the increase in serum full-length FGF23 in Fam20C KO mice and in humans with *FAM20C* mutations, namely reduced Fam20C phosphorylation allowing O-glycosylation and stabilization of FGF23.

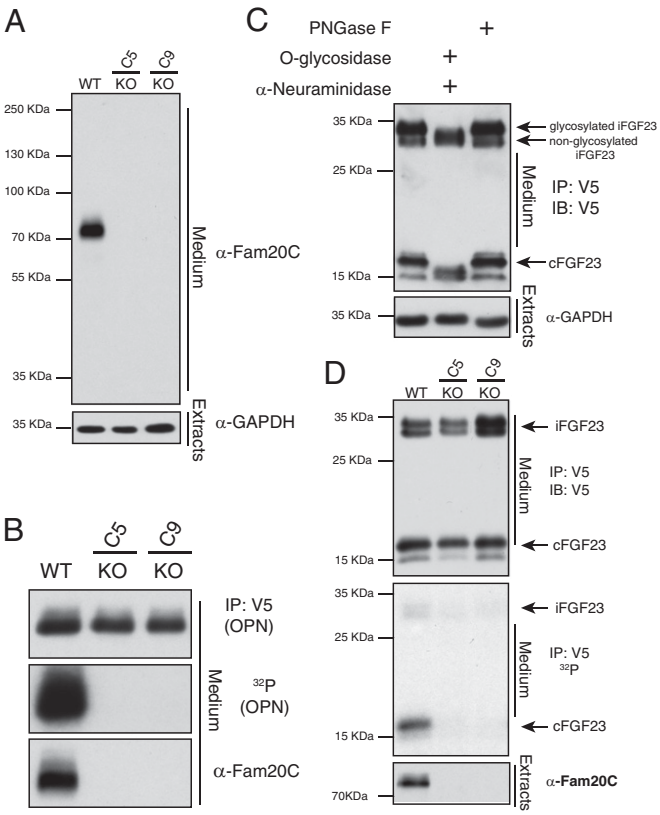

Fig. 2. Fam20C phosphorylates FGF23 in mammalian cells (*A*) Protein immunoblotting of trichloroacetic acid precipitates from conditioned medium of control and Fam20C KO cells (C5, clone 5; C9, clone 9) using an affinity-purified rabbit anti-Fam20C polyclonal antibody. GAPDH from cell extracts is shown as loading control (*Lower*). (*B*) Control and Fam20C KO cells were metabolically labeled with $^{32}PO_4^{3-}$ and transfected with V5-tagged OPN. Protein immunoblotting of V5-immunoprecipitates from conditioned medium (*Top*) and autoradiography depicting ^{32}P incorporation into OPN (*Middle*). Fam20C protein levels in conditioned medium are also shown (*Bottom*). (*C*) Protein immunoblotting of V5-immunoprecipitates from the conditioned medium of U2OS cells expressing V5-tagged FGF23. V5-immunoprecipitates were treated with O-glycosidase and α-(2→3,6,8,9)-neuraminidase to remove O-linked glycosylation or PNGase F to remove N-linked glycosylation. (*D*) Control and Fam20C KO cells were metabolically labeled with $^{32}PO_4^{3-}$ and transfected with V5-tagged FGF23. Protein immunoblotting of V5-immunoprecipitates from conditioned medium (*Top*) and autoradiography depicting ^{32}P incorporation into FGF23 (*Middle*). Intact FGF23 and C-terminal fragments are shown. Fam20C protein levels in conditioned medium are also shown (*Bottom*). IB, immunoblotting; IP, immunoprecipitation.

Phosphorylated FGF23 Is Cleaved by the SPC Furin. The importance of FGF23 cleavage is underscored in patients with ADHR who have mutations that substitute the Arg residues within the SPC cleavage site and render the protein resistant to proteolysis (Fig. 1*A*) (24, 25). As our above results support, phosphorylation of FGF23 at Ser^{180} inhibits O-glycosylation and would therefore promote hormone proteolysis and thus inactivation. The specific protease that inactivates FGF23 has yet to be conclusively identified, but is likely a member of the SPC family based upon

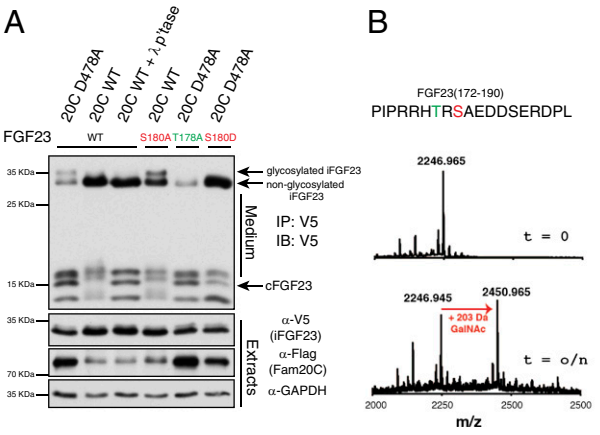

Fig. 3. Phosphorylation of FGF23 at Ser^{180} inhibits O-glycosylation by GalNAc-T3. (*A*) Protein immunoblotting of V5-immunoprecipitates from the conditioned medium of U2OS cells expressing V5-tagged FGF23 or mutants (S180A, T178A, S180D) with either WT (20C) or catalytically inactive D478A (20C D478A) FLAG-tagged Fam20C. V5-immunoprecipitates were treated with λ-phosphatase (λp'tase) (*Upper*). Extracts were analyzed for Fam20C, Fam20C D478A, FGF23, and GAPDH (*Lower*). (*B* and *C*) sGalNAc-T3 was incubated overnight (o/n) with FGF23(172–190) (*B*) or Ser^{180}-phosphorylated FGF23(172–190) (*C*) and UDP-GalNAc. The products were analyzed by MALDI-TOF MS.

the RXXR sequence comprising the cleavage site. With respect to our model, the protease must cleave FGF23 between Arg^{179} and a phosphorylated Ser^{180} (^{176}RHTR↓pSAE^{182}). To explore the proteolytic processing of phosphorylated FGF23, we coexpressed Flag-tagged PCSK1, PCSK2, and PCSK3 (furin) with V5-tagged FGF23 in U2OS cells. Coexpression of the proteases and FGF23 had no detectable effect on the relative levels of full-length secreted WT FGF23 (Fig. 4*A*). However, when FGF23 S180D (a phosphomimetic residue) or T178A (an O-glycosylation–defective mutant) was coexpressed with the proteases, the SPC furin completely abolished the iFGF23 but did not concurrently increase the levels of the C-terminal fragments (Fig. 4*A*). We reasoned that this could potentially be due to the presence of additional furin-specific RXXR recognition motifs within the C terminus of FGF23 that are cleaved by overexpressed furin. Therefore, to resolve this experimental possibility, we deleted furin in U2OS cells using CRISPR/Cas9 genome editing (Fig. S7). When WT FGF23 was expressed in furin KO cells, only intact FGF23 was detected, suggesting that furin cleaves FGF23 (Fig. 4*B*). Moreover, we analyzed the ability of recombinant furin to cleave the Ser^{180}-phosphorylated FGF23 (172–190) peptide by MALDI-TOF MS. Incubation of the nonphosphorylated or phosphorylated peptide with furin resulted in the time-dependent cleavage of both substrates (Fig. 4 *C* and *D* and Fig. S8). Thus, phosphorylation of FGF23 at Ser^{180} prevents Thr^{178} O-glycosylation by GalNAc-T3, which then allows furin-dependent proteolysis.

Incomplete Inhibition of FGF23 O-Glycosylation by Fam20C T268M. Raine syndrome was originally described in 1989 as an aggressive, neonatal osteosclerotic bone dysplasia that results in death within the first few weeks of life (11). Subsequently, mutations in the *FAM20C* gene were found to be responsible for this disorder (10), and recent reports suggest a broader phenotypic spectrum for individuals with *FAM20C* mutations because some patients survive infancy (12, 34). Notably, Rafaelsen et al. (12) identified a novel missense mutation in Fam20C that substituted Thr^{268} with a Met in two compound heterozygous brothers who had elevated serum intact FGF23 and hypophosphatemia. Threonine 268 (Thr^{175} in *Caenorhabditis elegans*) is highly conserved within the Fam20C subfamily, and the *C. elegans* Fam20 crystal structure revealed that this Thr is located in the glycine-rich loop (β1-β2), a region important for nucleotide binding (35) (Fig. 5 *A* and *B*). To test the impact of this mutation on FGF23 phosphorylation and O-glycosylation, we generated Flag-tagged Fam20C with Thr^{268} mutated to Met (Fam20C T268M) and analyzed its activity as well as the ability to be secreted from U2OS cells. In contrast to other nonlethal Fam20C mutations (3), substitution of Thr^{268} with Met did not affect Fam20C secretion (Fig. 5 *C* and *D*). Fam20C T268M phosphorylated OPN and FGF23 much less efficiently than WT Fam20C, as judged by its ability to induce a mobility change in OPN (Fig. 5*C*) and the secreted, C-terminal fragment of FGF23 (Fig. 5*D*). Importantly, expression of Fam20C T268M did not completely prevent O-glycosylation of intact FGF23, whereas WT Fam20C achieved complete inhibition of FGF23 O-glycosylation (Fig. 5*D*). Taken together, these findings support that the elevated intact FGF23 and hypophosphatemia observed in patients with the Fam20C T268M mutation are a result of the inability of Fam20C to efficiently phosphorylate FGF23 to inhibit O-glycosylation. As a consequence, elevated biologically active, O-linked glycosylated FGF23 is secreted, ultimately resulting in hypophosphatemia.

Discussion

The results of this study expand our understanding of the complex control of mammalian phosphate homeostasis. Our model for the regulation of FGF23 envisions a highly dynamic interplay between O-glycosylation by GalNAc-T3 (or other members of the GalNAc-transferase family) and phosphorylation by Fam20C as a means by which to balance the processing of FGF23 as intact, biologically active protein (glycosylated > phosphorylated) or N- and C-terminal fragments (phosphorylated > glycosylated) (Fig. S9). This model is consistent with the marked elevation of intact, biologically active FGF23 observed in humans with the Fam20C T268M mutation (12) and in *Fam20C* KO mice (13, 14).

Sensing the need to adapt phosphate balance in vivo is a complex process, and our data support that the production of bioactive FGF23 will depend upon, in addition to the levels of FGF23 transcription, the relative expression and activities of osteoblast/osteocyte Fam20C, GalNAc-T3, and furin. The mechanisms by which Fam20C is functionally or expressionally regulated are unknown. Recent studies examining the production of intact and/or C-terminal fragments of FGF23 in fibrous dysplasia and during physiological situations of low iron, such as in ADHR (36, 37), support that GalNAc-T3 and furin are likely controlled by multiple factors including 3′,5′-cyclic adenosine monophosphate (38), iron or iron deficiency (39), and inorganic phosphate (40).

Site-specific O-glycosylation within, or neighboring, SPC sites is emerging as an important regulatory mechanism to control SPC-dependent processing of secreted proteins (41). Our results are in accord with the concept that phosphorylation of hormones may promote proteolysis by SPCs (or other proteases) by interfering with O-glycosylation by members of the GalNAc-transferase family. Our observation of competition between phosphorylation and O-glycosylation in the secretory pathway reflects prior observations on the cross-talk between phosphorylation and O-glycosylation by O-linked *N*-acetylglucosamine (O-GlcNAc) transferase, which transfers GlcNAc from UDP-GlcNAc to Ser and Thr residues in nuclear and cytosolic proteins (42). Interplay between O-glycosylation and phosphorylation of the tumor suppressor p53 has been shown to coordinately regulate p53 stability and activity (43). Analogous

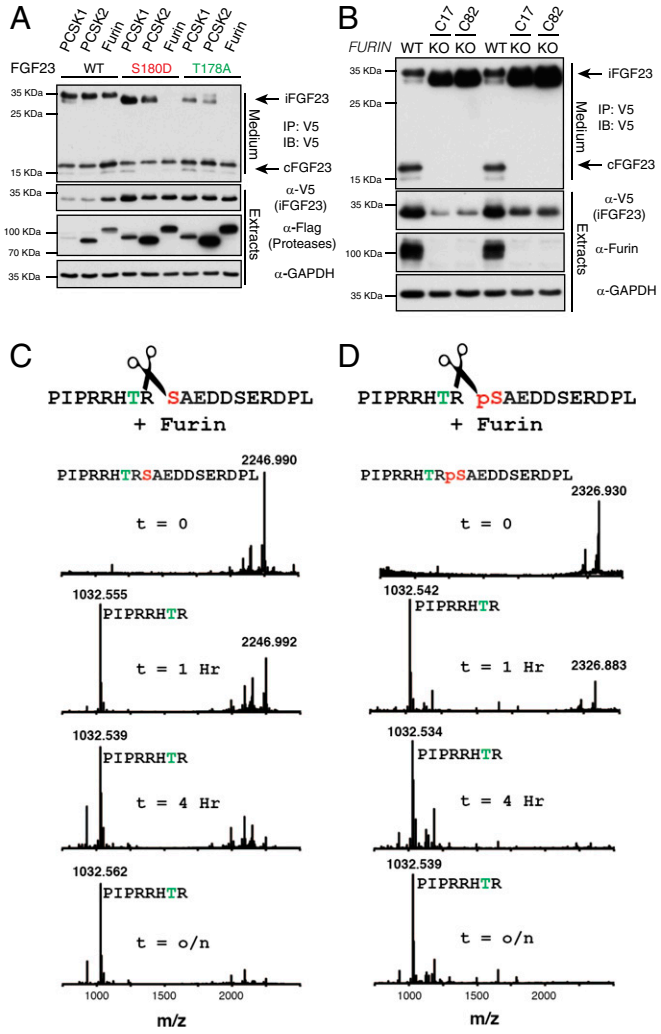

Fig. 4. Furin cleaves phosphorylated FGF23. (*A*) Protein immunoblotting of V5-immunoprecipitates from the conditioned medium of U2OS cells expressing V5-tagged FGF23 or mutants (S180D and T178A) with FLAG-tagged PCSK1, PCSK2, or PCSK3 (furin) (*Upper*). Extracts were analyzed for PCSK1–3, FGF23, and GAPDH expression (*Lower*). (*B*) Protein immunoblotting of V5-immunoprecipitates from the conditioned medium of control or *FURIN* KO U2OS cells (C17, clone 17; C82, clone 82) (*Upper*). Extracts were analyzed for FGF23 and GAPDH expression (*Lower*). (*C* and *D*) Time-dependent cleavage of FGF23(172–190) (*C*) or Ser^{180}-phosphorylated FGF23(172–190) (*D*). The products were analyzed by MALDI-TOF MS.

to what we observed in this work, phosphorylation of p53 promotes its degradation by the ubiquitin system by inhibiting O-GlcNAcylation. Currently, it is unknown whether the interplay between O-glycosylation by members of the GalNAc-transferase family and phosphorylation by secretory pathway kinases is a common mechanism within the secretory pathway or whether FGF23 is a unique example. However, it is worth noting that bone morphogenetic protein 15 (BMP15), a secreted maternal hormone essential for mammalian reproduction, is phosphorylated by Fam20C on an S-x-E motif (44). This phosphorylation site (Ser^{6}) is located close to an O-glycosylated Thr (Thr^{10}). When BMP15 is expressed in HEK293 cells, phosphorylation and O-glycosylation appear to be mutually exclusive (45).

The physiological scenario for the regulated control of circulating FGF23 is likely far more complicated than direct interactions between FGF23, Fam20C, GalNAc-T3, and furin. It is possible that Fam20C regulates FGF23 not only through direct mechanisms, as our results suggest, but also through emerging, indirect pathways. In this regard, we have shown that DMP1, a highly phosphorylated extracellular matrix protein critical for proper mineralization of bone (46), is a substrate for Fam20C (3, 4). Inactivating mutations in DMP1 result in autosomal recessive hypophosphatemic rickets, and *Dmp1* KO mice share many phenotypic similarities with those of *Fam20C*-deficient animals, including elevated FGF23 (13, 22). DMP1 appears to regulate FGF23 expression indirectly, as loss of Dmp1 in vivo impairs the maturation of osteoblasts to osteocytes through unknown mechanisms and results in highly elevated FGF23 mRNA as well as circulating protein (22). Thus, loss of DMP1 phosphorylation in a state of Fam20C deficiency could also contribute to an increase in FGF23 in vivo. Certainly additional studies will be required to understand these new interactions.

In addition to Ser^{180}, three Fam20C consensus S-x-E/pS sites are present in the C-terminal fragment of FGF23 (residues 180–250). We were unable to detect FGF23 peptides surrounding the predicted sites by MS, and therefore at this time we cannot rule out Fam20C-dependent phosphorylation of these residues. By quantitating the incorporated radioactivity in Fig. 1*D*, we calculated a stoichiometry of about 1.5–2 mol of phosphate per mol FGF23 R176Q, suggesting that other sites may be phosphorylated.

In conclusion, we have demonstrated that Fam20C regulates FGF23 by phosphorylation of Ser^{180}. Phosphorylation of FGF23 inhibits GalNAc-T3 O-glycosylation, which then allows proteolysis by furin. Collectively, our results provide a mechanism by which loss of Fam20C leads to aberrations in phosphate homeostasis due to a cellular shift toward increased O-glycosylation and thus elevated levels of intact, biologically active FGF23 and, conversely, increased Fam20C activity shifts the FGF23 processing balance toward increased furin proteolysis and hormone inactivation. Furthermore, our data suggest that interplay between phosphorylation and O-glycosylation of proteins in the secretory

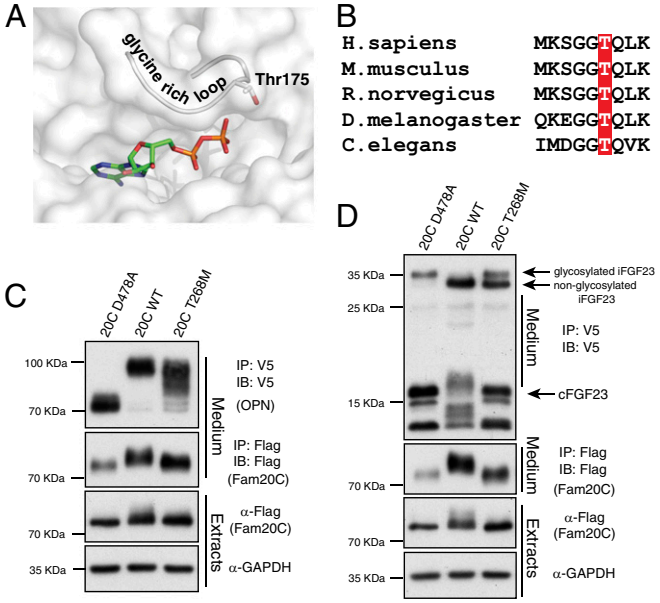

Fig. 5. Deficient inhibition of FGF23 O-glycosylation by Fam20C T268M. (*A*) Structural representation of the active site of Fam20 from *C. elegans* highlighting the position of Thr^{175} (human Thr^{268}). The glycine-rich loop and nucleotide (ADP) are shown. (*B*) Sequence alignment of Fam20C from human (*Homo sapiens*), mouse (*Mus musculus*), rat (*Rattus norvegicus*), fly (*Drosophila melanogaster*), and worm (*Caenorhabditis elegans*) depicting the conservation of the Thr. (*C* and *D*) Protein immunoblotting of V5 and Flag-immunoprecipitates from conditioned medium of U2OS cells expressing V5-tagged OPN (*C*) or FGF23 (*D*) with Flag-tagged D478A (20C D478A), WT (20C WT), or mutant Fam20C found in patients with FGF23-related hypophosphatemia (20C T268M) (*Upper*). Extracts were analyzed for Fam20C and GAPDH expression (*Lower*).

pathway may be a critical posttranslational mechanism by which secreted proteins are regulated.

Methods

Protein Purification. Flag-tagged Fam20C and FGF23 R176Q were immunopurified from conditioned medium of HEK293T cells as previously described (3). More details on protein purification are presented in *SI Methods*.

Generation of Anti-Fam20C Antibody. Polyclonal antisera were raised in rabbits against recombinant Flag-tagged Fam20C produced in HEK293T cells (Cocalico Biologicals). More details on antibody generation are presented in *SI Methods*.

ACKNOWLEDGMENTS. We thank Carolyn A. Worby, Gregory S. Taylor, Jenna L. Jewell, and members of the J.E.D. laboratory for insightful discussions and comments regarding the manuscript. We thank David King of the Howard Hughes Medical Institute's Mass Spectrometry Laboratory (University of California, Berkeley) for peptide synthesis and Eric Durrant for technical assistance. This work was supported in part by National Institutes of Health Grants DK018849-36 and DK018024-37 (to J.E.D.), DK63934 (to K.E.W.), and K99DK099254 (to V.S.T.).

1. Cohen P (2002) The origins of protein phosphorylation. *Nat Cell Biol* 4(5):E127–E130.
2. Fischer EH (2013) Cellular regulation by protein phosphorylation. *Biochem Biophys Res Commun* 430(2):865–867.
3. Tagliabracci VS, et al. (2012) Secreted kinase phosphorylates extracellular proteins that regulate biomineralization. *Science* 336(6085):1150–1153.
4. Ishikawa HO, Xu A, Ogura E, Manning G, Irvine KD (2012) The Raine syndrome protein FAM20C is a Golgi kinase that phosphorylates bio-mineralization proteins. *PLoS ONE* 7(8):e42988.
5. Tagliabracci VS, Pinna LA, Dixon JE (2013) Secreted protein kinases. *Trends Biochem Sci* 38(3):121–130.
6. Tagliabracci VS, Xiao J, Dixon JE (2013) Phosphorylation of substrates destined for secretion by the Fam20 kinases. *Biochem Soc Trans* 41(4):1061–1065.
7. Salvi M, Cesaro L, Tibaldi E, Pinna LA (2010) Motif analysis of phosphosites discloses a potential prominent role of the Golgi casein kinase (GCK) in the generation of human plasma phospho-proteome. *J Proteome Res* 9(6):3335–3338.
8. Zhou W, et al. (2009) An initial characterization of the serum phosphoproteome. *J Proteome Res* 8(12):5523–5531.
9. Bahl JM, Jensen SS, Larsen MR, Heegaard NH (2008) Characterization of the human cerebrospinal fluid phosphoproteome by titanium dioxide affinity chromatography and mass spectrometry. *Anal Chem* 80(16):6308–6316.
10. Simpson MA, et al. (2007) Mutations in FAM20C are associated with lethal osteosclerotic bone dysplasia (Raine syndrome), highlighting a crucial molecule in bone development. *Am J Hum Genet* 81(5):906–912.
11. Raine J, Winter RM, Davey A, Tucker SM (1989) Unknown syndrome: Microcephaly, hypoplastic nose, exophthalmos, gum hyperplasia, cleft palate, low set ears, and osteosclerosis. *J Med Genet* 26(12):786–788.
12. Rafaelsen SH, et al. (2013) Exome sequencing reveals FAM20c mutations associated with FGF23-related hypophosphatemia, dental anomalies and ectopic calcification. *J Bone Miner Res* 28(6):1378–1385.
13. Wang X, et al. (2012) Inactivation of a novel FGF23 regulator, FAM20C, leads to hypophosphatemic rickets in mice. *PLoS Genet* 8(5):e1002708.
14. Vogel P, et al. (2012) Amelogenesis imperfecta and other biomineralization defects in Fam20a and Fam20c null mice. *Vet Pathol* 49(6):998–1017.
15. Bhattacharyya N, Chong WH, Gafni RI, Collins MT (2012) Fibroblast growth factor 23: State of the field and future directions. *Trends Endocrinol Metab* 23(12):610–618.
16. Farrow EG, White KE (2010) Recent advances in renal phosphate handling. *Nat Rev Nephrol* 6(4):207–217.
17. Kurosu H, et al. (2006) Regulation of fibroblast growth factor-23 signaling by klotho. *J Biol Chem* 281(10):6120–6123.
18. Carpenter TO (2012) The expanding family of hypophosphatemic syndromes. *J Bone Miner Metab* 30(1):1–9.
19. Liu S, et al. (2006) Pathogenic role of Fgf23 in Hyp mice. *Am J Physiol Endocrinol Metab* 291(1):E38–E49.
20. Consortium TH; The HYP Consortium (1995) A gene (PEX) with homologies to endopeptidases is mutated in patients with X-linked hypophosphatemic rickets. *Nat Genet* 11(2):130–136.
21. Lorenz-Depiereux B, Schnabel D, Tiosano D, Häusler G, Strom TM (2010) Loss-of-function ENPP1 mutations cause both generalized arterial calcification of infancy and autosomal-recessive hypophosphatemic rickets. *Am J Hum Genet* 86(2):267–272.
22. Feng JQ, et al. (2006) Loss of DMP1 causes rickets and osteomalacia and identifies a role for osteocytes in mineral metabolism. *Nat Genet* 38(11):1310–1315.
23. Bergwitz C, Jüppner H (2010) Regulation of phosphate homeostasis by PTH, vitamin D, and FGF23. *Annu Rev Med* 61:91–104.
24. White KE, et al. (2000) Autosomal dominant hypophosphataemic rickets is associated with mutations in FGF23. *Nat Genet* 26(3):345–348.
25. White KE, et al. (2001) Autosomal-dominant hypophosphatemic rickets (ADHR) mutations stabilize FGF-23. *Kidney Int* 60(6):2079–2086.
26. Benet-Pagès A, Orlik P, Strom TM, Lorenz-Depiereux B (2005) An FGF23 missense mutation causes familial tumoral calcinosis with hyperphosphatemia. *Hum Mol Genet* 14(3):385–390.
27. Topaz O, et al. (2004) Mutations in GALNT3, encoding a protein involved in O-linked glycosylation, cause familial tumoral calcinosis. *Nat Genet* 36(6):579–581.
28. Kato K, et al. (2006) Polypeptide GalNAc-transferase T3 and familial tumoral calcinosis. Secretion of fibroblast growth factor 23 requires O-glycosylation. *J Biol Chem* 281(27):18370–18377.
29. Bergwitz C, et al. (2009) Defective O-glycosylation due to a novel homozygous S129P mutation is associated with lack of fibroblast growth factor 23 secretion and tumoral calcinosis. *J Clin Endocrinol Metab* 94(11):4267–4274.
30. Wang X, et al. (2010) Expression of FAM20C in the osteogenesis and odontogenesis of mouse. *J Histochem Cytochem* 58(11):957–967.
31. Cong L, et al. (2013) Multiplex genome engineering using CRISPR/Cas systems. *Science* 339(6121):819–823.
32. Jinek M, et al. (2012) A programmable dual-RNA-guided DNA endonuclease in adaptive bacterial immunity. *Science* 337(6096):816–821.
33. Gill DJ, Clausen H, Bard F (2011) Location, location, location: New insights into O-GalNAc protein glycosylation. *Trends Cell Biol* 21(3):149–158.
34. Simpson MA, et al. (2009) Mutations in FAM20C also identified in non-lethal osteosclerotic bone dysplasia. *Clin Genet* 75(3):271–276.
35. Xiao J, Tagliabracci VS, Wen J, Kim SA, Dixon JE (2013) Crystal structure of the Golgi casein kinase. *Proc Natl Acad Sci USA* 110(26):10574–10579.
36. Farrow EG, et al. (2011) Iron deficiency drives an autosomal dominant hypophosphatemic rickets (ADHR) phenotype in fibroblast growth factor-23 (Fgf23) knock-in mice. *Proc Natl Acad Sci USA* 108(46):E1146–E1155.
37. Imel EA, et al. (2011) Iron modifies plasma FGF23 differently in autosomal dominant hypophosphatemic rickets and healthy humans. *J Clin Endocrinol Metab* 96(11):3541–3549.
38. Bhattacharyya N, et al. (2012) Mechanism of FGF23 processing in fibrous dysplasia. *J Bone Miner Res* 27(5):1132–1141.
39. Knutson MD (2010) Iron-sensing proteins that regulate hepcidin and enteric iron absorption. *Annu Rev Nutr* 30:149–171.
40. Chefetz I, et al. (2009) GALNT3, a gene associated with hyperphosphatemic familial tumoral calcinosis, is transcriptionally regulated by extracellular phosphate and modulates matrix metalloproteinase activity. *Biochim Biophys Acta* 1792(1):61–67.
41. Schjoldager KT, Clausen H (2012) Site-specific protein O-glycosylation modulates proprotein processing—Deciphering specific functions of the large polypeptide GalNAc-transferase gene family. *Biochim Biophys Acta* 1820(12):2079–2094.
42. Hart GW, Slawson C, Ramirez-Correa G, Lagerlof O (2011) Cross talk between O-GlcNAcylation and phosphorylation: Roles in signaling, transcription, and chronic disease. *Annu Rev Biochem* 80:825–858.
43. Yang WH, et al. (2006) Modification of p53 with O-linked *N*-acetylglucosamine regulates p53 activity and stability. *Nat Cell Biol* 8(10):1074–1083.
44. Tibaldi E, et al. (2010) Golgi apparatus casein kinase phosphorylates bioactive Ser-6 of bone morphogenetic protein 15 and growth and differentiation factor 9. *FEBS Lett* 584(4):801–805.
45. Saito S, Yano K, Sharma S, McMahon HE, Shimasaki S (2008) Characterization of the post-translational modification of recombinant human BMP-15 mature protein. *Protein Sci* 17(2):362–370.
46. George A, Veis A (2008) Phosphorylated proteins and control over apatite nucleation, crystal growth, and inhibition. *Chem Rev* 108(11):4670–4693.

Supporting Information

Tagliabracci et al. 10.1073/pnas.1402218111

SI Methods

Molecular Biology, Cell Culture, and Transfection. Human cDNAs for FGF23, PCSK1, PCSK3 (furin), and the family with sequence similarity 20, member C (Fam20C) were from Open Biosystems. Human PCSK2 and *N*-acetylgalactosaminyltransferase 3 (GalNAc-T3) cDNAs were from DNASU. The ORFs were amplified by PCR and cloned into mammalian expression plasmids containing a C-terminal V5/His tag (pcDNA4.0; Invitrogen) or a C-terminal Flag tag (pCCF). QuikChange site-directed mutagenesis (Agilent Technologies) was performed to introduce mutations. U2OS and HEK293T cells were grown in DMEM containing 10% (vol/vol) FBS with 100 μg/mL penicillin/streptomycin (GIBCO) at 37 °C with 5% CO_2. For coexpression experiments, 5×10^5 cells were seeded in 2 mL in a six-well plate format. Approximately 24 h later, cells were transfected with 0.5 μg pCCF-PCSK1/2/3 or pCCF-Fam20C (or mutants) and 2 μg pcDNA4.0-FGF23 (or mutants) with 7 μL FuGENE 6 (Roche) as recommended by the manufacturer. Forty to 48 h after transfection, the conditioned medium and cell extracts were harvested and analyzed.

Protein Immunoblotting and Immunoprecipitations. V5- and Flag-tagged proteins were analyzed by immunoprecipitation and immunoblotting as described (1). Furin protein was analyzed by immunoblotting cell extracts with an anti-furin polyclonal antibody (1:1,000 dilution; GeneTex). To detect Fam20C protein in conditioned medium, cells were extensively washed with PBS and serum-free DMEM and then incubated for a minimum of 16 h in serum-free DMEM. The medium was centrifuged at 750 × *g* for 5 min to remove cell debris. The supernatant was further centrifuged at 10,000 × *g* for 10 min, and 100% trichloroacetic acid (one-quarter the volume of the medium) was added to the resulting supernatant. The proteins were precipitated overnight at 4 °C and washed two or three times with −20 °C acetone. The samples were dried in a SpeedVac and resuspended in 1× SDS loading buffer. Fam20C protein was analyzed by immunoblotting with a rabbit polyclonal anti-Fam20C antibody.

Generation of Anti-Fam20C Antibody. Anti-Fam20C antibodies were affinity-purified by coupling maltose-binding protein (MBP) fusion peptides to HiTrap NHS-activated HP columns (GE Healthcare). The N-terminal MBP-fusion peptides (residues 20–361, 381–496, 423–584, and 381–584 of human Fam20C) were produced in *Escherichia coli* and affinity-purified using amylose resin (New England Biolabs).

Metabolic Radiolabeling of U2OS Cells. For metabolic radiolabeling experiments, 5×10^5 cells were seeded in 2 mL in a six-well plate format. Approximately 24 h later, cells were transfected with 5 μg of pcDNA4.0-FGF23 or pcDNA4.0-osteopontin with 10 μL FuGENE 6. Forty to 48 h after transfection, the medium was replaced with phosphate-free DMEM containing 10% (vol/vol) dialyzed FBS and 1 mCi/mL [^{32}P]orthophosphate (PerkinElmer). The cells were incubated for an additional 6–8 h at which time the conditioned medium was centrifuged at 750 × *g* for 5 min to remove cell debris. The medium was further centrifuged at 10,000 × *g* for 10 min and V5-tagged proteins were immunoprecipitated from the supernatant, washed five times with PBS containing 0.4 mM EDTA and 1% Nonidet P-40, and then analyzed for protein and incorporated ^{32}P by immunoblotting and autoradiography.

Clustered Regularly Interspaced Short Palindromic Repeats/Cas9 Genome Editing. The 20-nt guide sequences targeting human *FAM20C* and *FURIN* were designed using the clustered regularly interspaced short palindromic repeats (CRISPR) design tool at www.genome-engineering.org/crispr (2) and cloned into a bicistronic expression vector (pX330) containing human codon-optimized Cas9 and the RNA components (2) (Addgene).

The guide sequences targeting exon 1 of human *FAM20C* and exon 7 of human *FURIN* are shown below.

FAM20C.

5′-GGGCTGCGCGCACGAACAGC-3′ (clone 5)

5′-CCGCCCCCGCAAGGCGCGCT-3′ (clone 9)

FURIN.

5′-TACACCACAGACACCGTTGT-3′ (clones 17 and 82)

The single-guide RNAs (sgRNAs) in the pX330 vector (4 μg) were mixed with EGFP (1 μg; Clontech) and cotransfected into U2OS cells using FuGENE 6. Twenty-four hours posttransfection, the cells were trypsinized, washed with PBS, and resuspended in fluorescence-activated cell sorting (FACS) buffer (PBS, 5 mM EDTA, 2% FBS, and 100 μg/mL penicillin/streptomycin). GFP-positive cells were single-cell–sorted by FACS (Human Embryonic Stem Cell Core, University of California, San Diego; BD Influx) into a 96-well plate format into DMEM containing 20% FBS and 100 μg/mL penicillin/streptomycin. Single clones were expanded and screened for Fam20C and furin by protein immunoblotting. Genomic DNA (gDNA) was purified from clones using the Quick-gDNA Prep Kit (Zymo Research), and the region surrounding the protospacer adjacent motif (PAM) was amplified with Q5 polymerase (New England Biolabs) using the following primers (linkers containing EcoRI and HindIII restriction sites are underlined).

FAM20C.

Forward: 5′-AAAAGAATTCTGGAGAGGAGCGCGCTGAGGATC-3′

Reverse: 5′-AAAAAAGCTTTCCGGGTTCTCCGCCGCTTTG-3′

FURIN.

Forward: 5′-AAAAGAATTCACTCAGGGGATGATGGGTGTC-3′

Reverse: 5′-AAAAAAGCTTAGAGAAGGAAAAAGAGAACACCTCC-3′

PCR products were purified using the DNA Clean & Concentrator Kit (Zymo Research) and cloned into pBluescript II KS+. To determine the indels of individual alleles, ∼10 bacterial colonies were expanded and the plasmid DNA was purified and sequenced.

Protein Purification. Flag-tagged Fam20C and FGF23 R176Q were immunopurified from conditioned medium of HEK293T cells as previously described (1). FGF23 R176Q was further purified by Superdex 200 size-exclusion chromatography. To generate a secreted form of GalNAc-T3 (sGalNAc-T3), the nucleotides encoding residues 38–633 of human GalNAc-T3 were cloned into a modified retroviral (pQCXIP; Clontech) vector containing an N-terminal interleukin 2 signal peptide and a C-terminal Flag

tag. Stable expression and purification of sGalNAc-T3 from conditioned medium were performed as described (1).

Enzyme Assays. ***Kinase assays.*** In vitro kinase assays were performed essentially as described (1). The reaction mixture contained 32.5 mM Tris·HCl (pH 7.5), 100 mM NaCl, 12.5% glycerol, 10 mM $MnCl_2$, 0.5 mM [γ-^{32}P]ATP (specific activity 100–500 cpm/pmol), 0.5 mg/mL FGF23 R176Q, and 20 μg/mL Fam20C-Flag or Fam20C (D478A)-Flag.

Glycosylation assays. In vitro O-glycosylation assays were performed essentially as described (3). Reactions were performed in a 20-μL mixture containing 25 mM sodium cacodylate (pH 7.4), 10 mM $MnCl_2$, 1.5 mM UDP-GalNAc (Sigma), 0.5 mg/mL peptide substrate: PIPRRHTRSAEDDSERDPL; FGF23(172–190) or PIPRRHTRpSAEDDSERDPL; pFGF23(172–190), and 50 μg/mL sGalNAc-T3. Reactions were incubated at 37 °C and terminated at the indicated time points by the addition of an equal volume of Sigma-Aldrich universal MALDI matrix resuspended in 78% acetonitrile and 0.1% trifluoroacetic acid.

Protease assays. Furin cleavage assays were performed as previously described (3). Reactions were performed in a 20-μL mixture containing 50 mM Hepes (pH 7.5), 1 mM $CaCl_2$, 0.5 mg/mL FGF23(172–190) or pFGF23(172–190), and 0.02 units per μL furin (New England Biolabs). Reactions were incubated at 37 °C and terminated at the indicated time points by the addition of an equal volume of Sigma-Aldrich universal MALDI matrix resuspended in 78% acetonitrile and 0.1% trifluoroacetic acid.

Deglycosylation and λ-phosphatase assays. V5-immunoprecipitates from conditioned medium of U2OS cells transiently expressing V5-tagged FGF23 were treated with O-glycosidase and α-(2→3,6,8,9)-neuraminidase to remove O-linked glycosylation or PNGase F to remove N-linked glycosylation according to the manufacturer's instructions (Sigma-Aldrich; Enzymatic Protein Deglycosylation Kit). λ-Phosphatase assays were performed as described (1).

Matrix-Assisted Laser Desorption/Ionization Analysis. Glycosylation and protease reaction products (1 μL) were plated on an Applied Biosciences (ABI) MALDI target plate for analysis. The ABI 4800 MALDI-TOF/TOF was calibrated at 25 ppm mass error with a peptide mix standard. After calibration, each spot was analyzed using reflectron positive ionization and a laser power of 30%. Masses that corresponded to truncated forms of peptide PIPRRHTRSAEDDSERDPL and the phosphorylated version PIPRRHTRpSAEDDSERDPL were sequenced de novo for validation. In addition, b- and y-ion masses were used to localize phosphorylated residues on fragment ions.

Peptide Synthesis. Peptides and phosphopeptides were synthesized by standard O-(Benzotriazol-1-yl)-N,N,N′,N′-tetramethyluronium hexafluorophosphate/1-Hydroxybenzotriazole (HBTU/HOBt) Fmoc solid-phase chemistry on Wang resin using an ABI 431A synthesizer and incorporating pSer as its Fmoc-*O*-benzyl ester. Peptide–resin was cleaved with reagent K (2-Ethyl-5-phenylisoxazolium-3′-sulfonate). Identity and purity were assessed by electrospray ionization-Fourier transform ion cyclotron resonance mass spectrometry; the purity of crude peptide was at least 90%. Peptides were dissolved in 10 mM Hepes and the pH was adjusted to 7 with NaOH before use.

Mass Spectrometry. Fifty picomoles of Flag-tagged FGF23 R176Q was oxidized with 4 mM DTT and alkylated with 8 mM iodoacetamide and digested with either trypsin, endoproteinase GluC, or chymotrypsin. The resulting peptide extract was diluted into a solution of 2% acetonitrile, 0.1% formic acid (buffer A) for analysis. Two picomoles of each digest was analyzed by automated microcapillary liquid chromatography-tandem mass spectrometry. Fused-silica capillaries (100-μm inner diameter; i.d.) were pulled using a P-2000 CO_2 laser puller (Sutter Instruments) to a 5-μm i.d. tip and packed with 10 cm of 5-μm Magic C18 material (Agilent) using a pressure bomb. This column was then installed in-line with a Dionex 3000 HPLC pump running at 300 nL/min. Peptides were loaded with an autosampler directly onto the column and were eluted from the column by applying a 30-min gradient from 5% buffer B to 40% buffer B (98% acetonitrile, 0.1% formic acid). The gradient was switched from 40% to 80% buffer B over 5 min and held constant for 3 min. Finally, the gradient was changed from 80% buffer B to 100% buffer A over 0.1 min, and then held constant at 100% buffer A for 15 more minutes. The application of a 1.8-kV distal voltage electrosprayed the eluting peptides directly into an LTQ XL ion trap mass spectrometer equipped with a nano-liquid chromatography electrospray ionization source. Full mass spectra were recorded on the peptides over 400–2,000 *m/z*, followed by five tandem mass (MS/MS) events on the five most intense ions. Mass spectrometer scan functions and HPLC solvent gradients were controlled by the Xcalibur data system (Thermo Finnigan). MS/MS spectra were extracted with ReAdW.exe (http://sourceforge.net/projects/sashimi). The resulting mzXML file contains all of the data for all MS/MS spectra and can be read by the subsequent analysis software. The MS/MS data were searched with Inspect (4) against a database containing protein sequences for all *E. coli* proteins, common contaminants, and the sequence for FGF23 R176Q (2,786 proteins) with modifications: +16 on methionine (oxidation), +57 on cysteine (carbamidomethyl), and + 80 on threonine, serine, or tyrosine (phosphorylation). Only peptides with at least a *P* value of 0.01 were analyzed further. The MS/MS data of putative phosphorylated peptides were manually verified. In addition, further verification was performed by analyzing putative phosphorylated peptides in targeted MS/MS mode.

1. Tagliabracci VS, et al. (2012) Secreted kinase phosphorylates extracellular proteins that regulate biomineralization. *Science* 336(6085):1150–1153.
2. Hsu PD, et al. (2013) DNA targeting specificity of RNA-guided Cas9 nucleases. *Nat Biotechnol* 31(9):827–832.
3. Kato K, et al. (2006) Polypeptide GalNAc-transferase T3 and familial tumoral calcinosis. Secretion of fibroblast growth factor 23 requires O-glycosylation. *J Biol Chem* 281(27): 18370–18377.
4. Tanner S, et al. (2005) InsPecT: Identification of posttranslationally modified peptides from tandem mass spectra. *Anal Chem* 77(14):4626–4639.

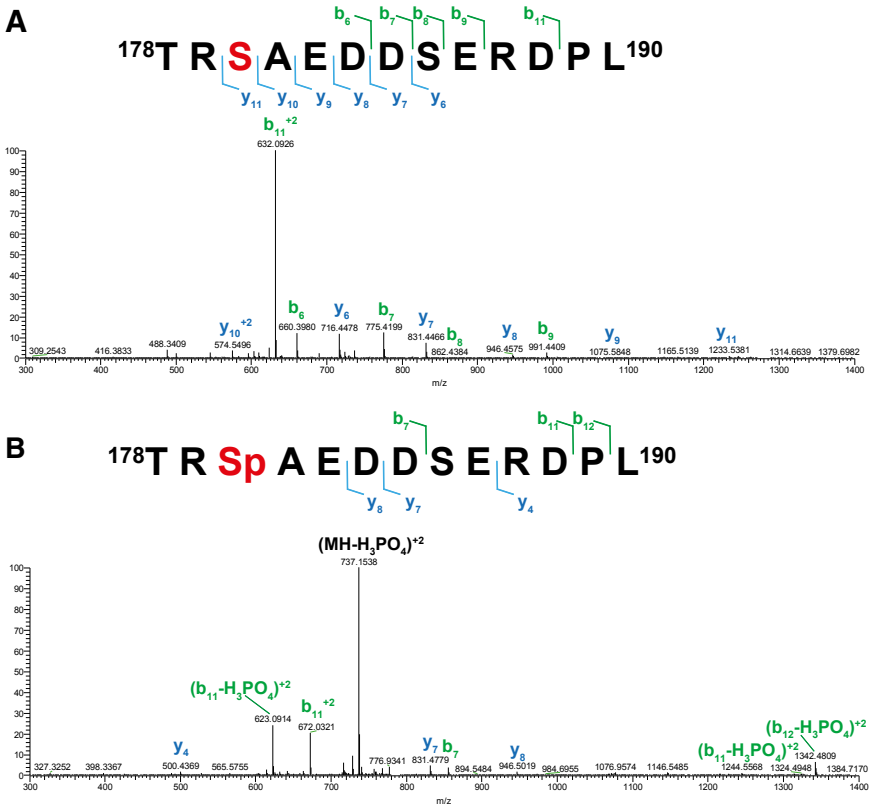

Fig. S1. FGF23 is phosphorylated on Ser[180]. Representative MS/MS fragmentation spectra of a chymotryptic peptide (FGF23 178–190) depicting Ser[180] phosphorylation of FGF23 R176Q purified from conditioned medium of HEK293T cells. The nonphosphopeptide and the phosphopeptide are shown in *A* and *B*, respectively.

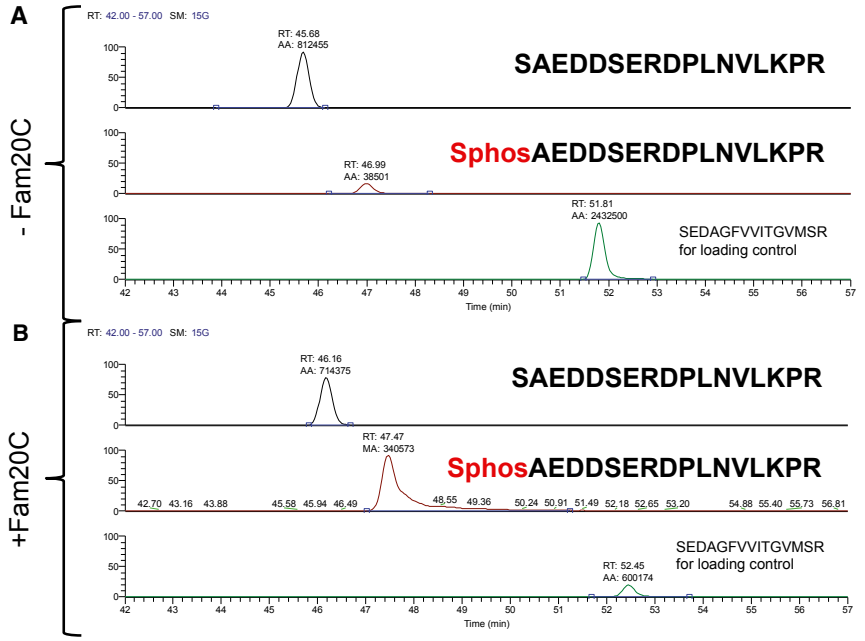

Fig. S2. Fam20C phosphorylates FGF23 on Ser[180]. Selected ion chromatograms of tryptic peptides (FGF23 180–196) from FGF23 R176Q (*A*) or FGF23 R176Q that had been treated with recombinant Fam20C (*B*). Note the relative 10-fold increase in the relative abundance of the phosphopeptide upon treatment with Fam20C. Calculations are estimated based on the areas under the curve for the selected ion species (AA phospho/nonphospho; 38,501/812,455 = 0.05; 340,573/714,375 = 0.5). AA and MA, area; RT, retention time.

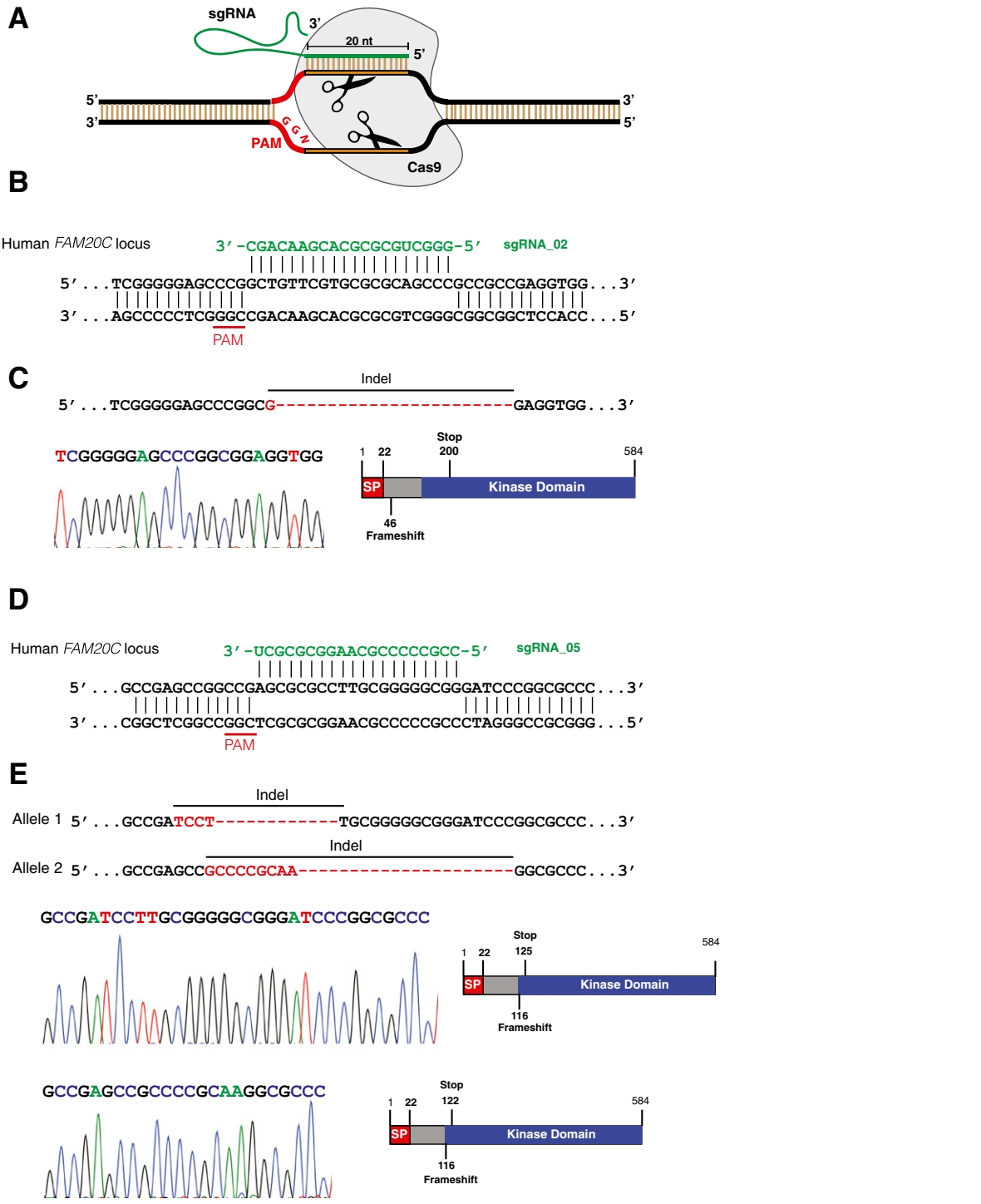

Fig. S3. Generation of Fam20C knockout cells using CRISPR/Cas9 genome editing. (*A*) The type II prokaryotic CRISPR/Cas9 from *Streptococcus pyogenes* has been shown to facilitate RNA-guided site-specific DNA cleavage and can be harnessed to target the destruction of specific genes in mammalian cells (1–3). Any genomic locus followed by a 5′-NGG PAM (red) can be targeted by a chimeric single guide RNA (sgRNA) (green) consisting of a 20-nt guide sequence and a scaffold. The sgRNA directs the Cas9 nuclease (gray) to the genomic target, resulting in a double-strand break. The double-strand break is repaired by error-prone nonhomologous end joining or by homologous recombination. (*B* and *D*) Schematic representations of the base pairing between guide RNAs and the targeting locus of exon 1 in the human *FAM20C* gene. (*C* and *E*) The sequences of the mutated alleles in *FAM20C* clone 5 (*C*) and clone 9 (*E*) and representative chromatograms depicting the indels (red) are shown. The indels are predicted to cause frameshift mutations producing inactive copies of the protein. SP, signal peptide.

1. Cong L, et al. (2013) Multiplex genome engineering using CRISPR/Cas systems. *Science* 339(6121):819–823.
2. Jinek M, et al. (2012) A programmable dual-RNA-guided DNA endonuclease in adaptive bacterial immunity. *Science* 337(6096):816–821.
3. Jinek M, et al. (2013) RNA-programmed genome editing in human cells. *Elife* 2:e00471.

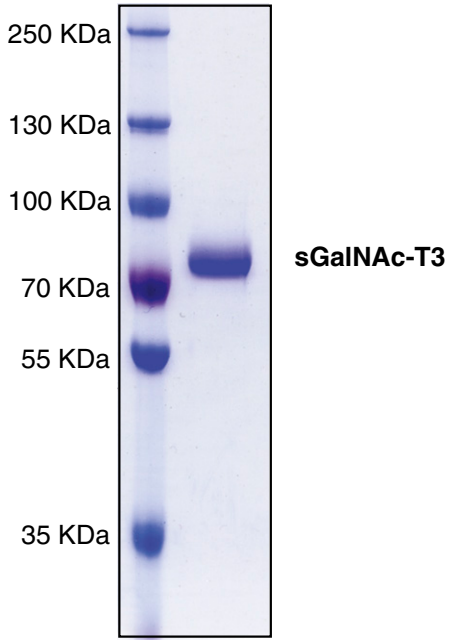

Fig. S4. Expression and purification of sGalNAc-T3. SDS/PAGE and Coomassie staining of Flag-tagged sGalNAc-T3 immunopurified from the conditioned medium of HEK293T cells.

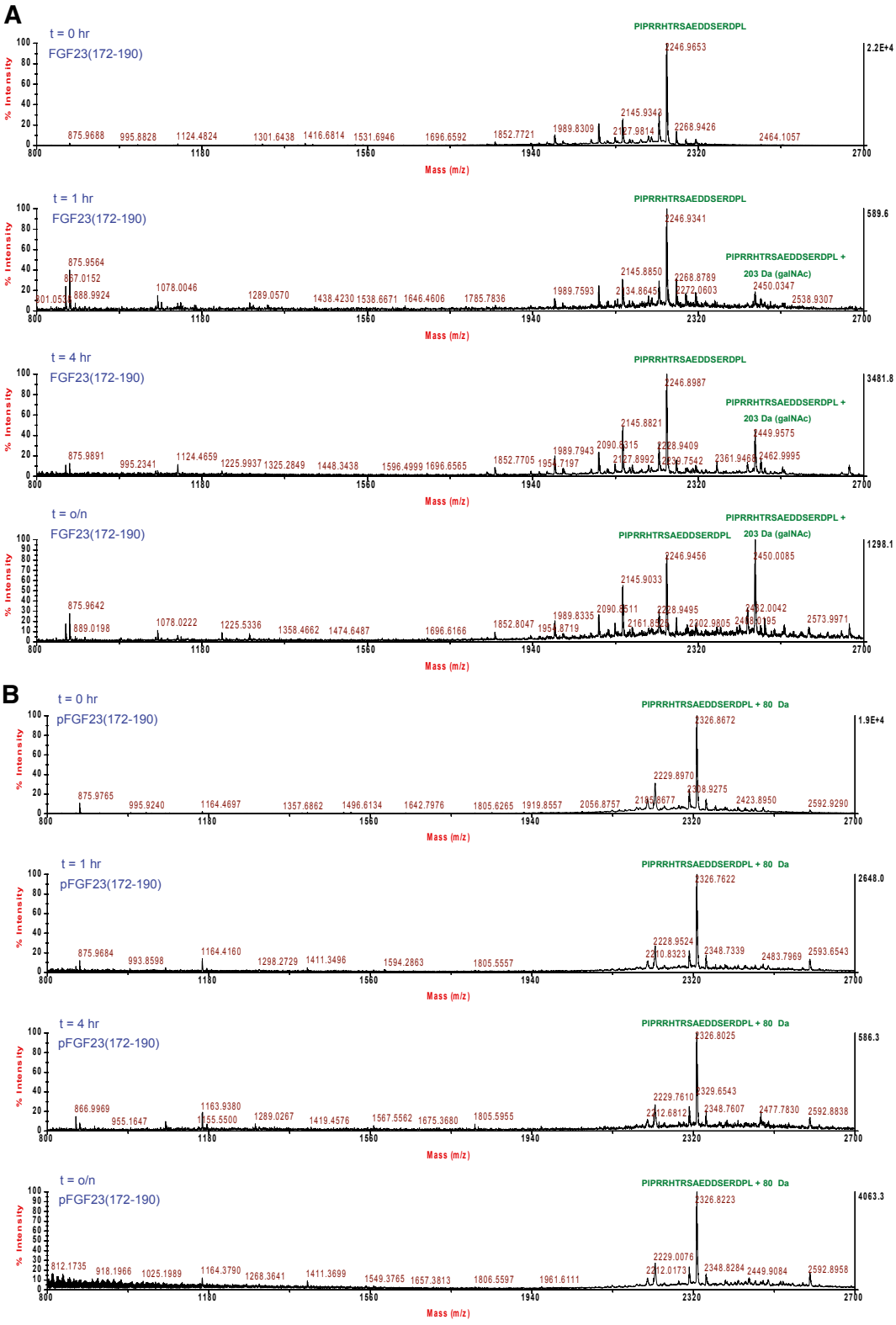

Fig. S5. Ser^{180}-phosphorylated FGF23(172–190) is not a substrate for sGalNAc-T3. Full MALDI-TOF MS spectra depicting the time-dependent incorporation of GalNAc from UDP-GalNAc into FGF23(172–190) (*A*) or Ser^{180}-phosphorylated FGF23(172–190) (*B*).

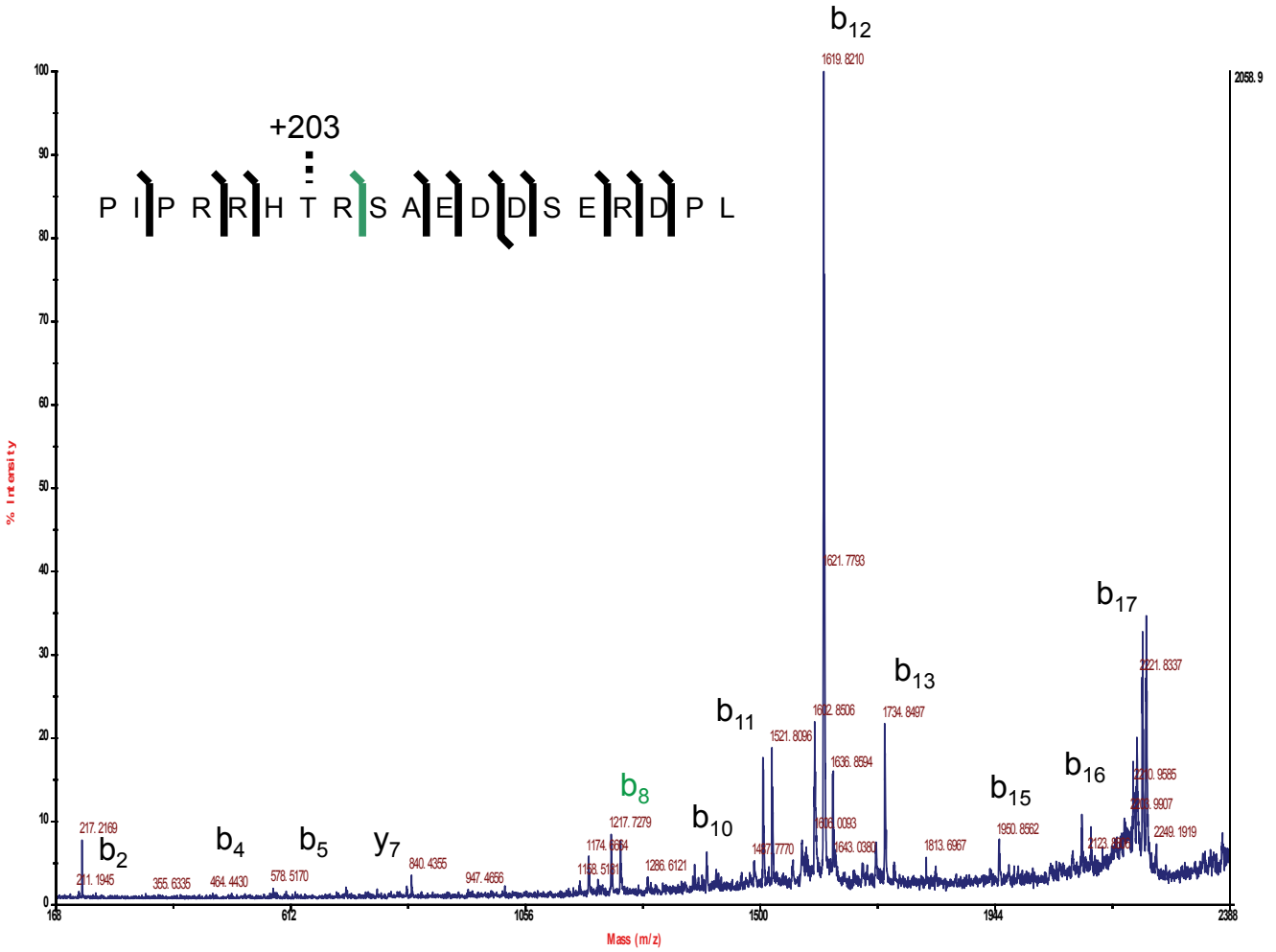

Fig. S6. Thr^{178} is O-glycosylated by sGalNAc-T3. Representative MS/MS fragmentation spectrum of the selected ion peak at *m/z* 2450 in Fig. S5*A*, depicting the addition of GalNAc to Thr^{178}.

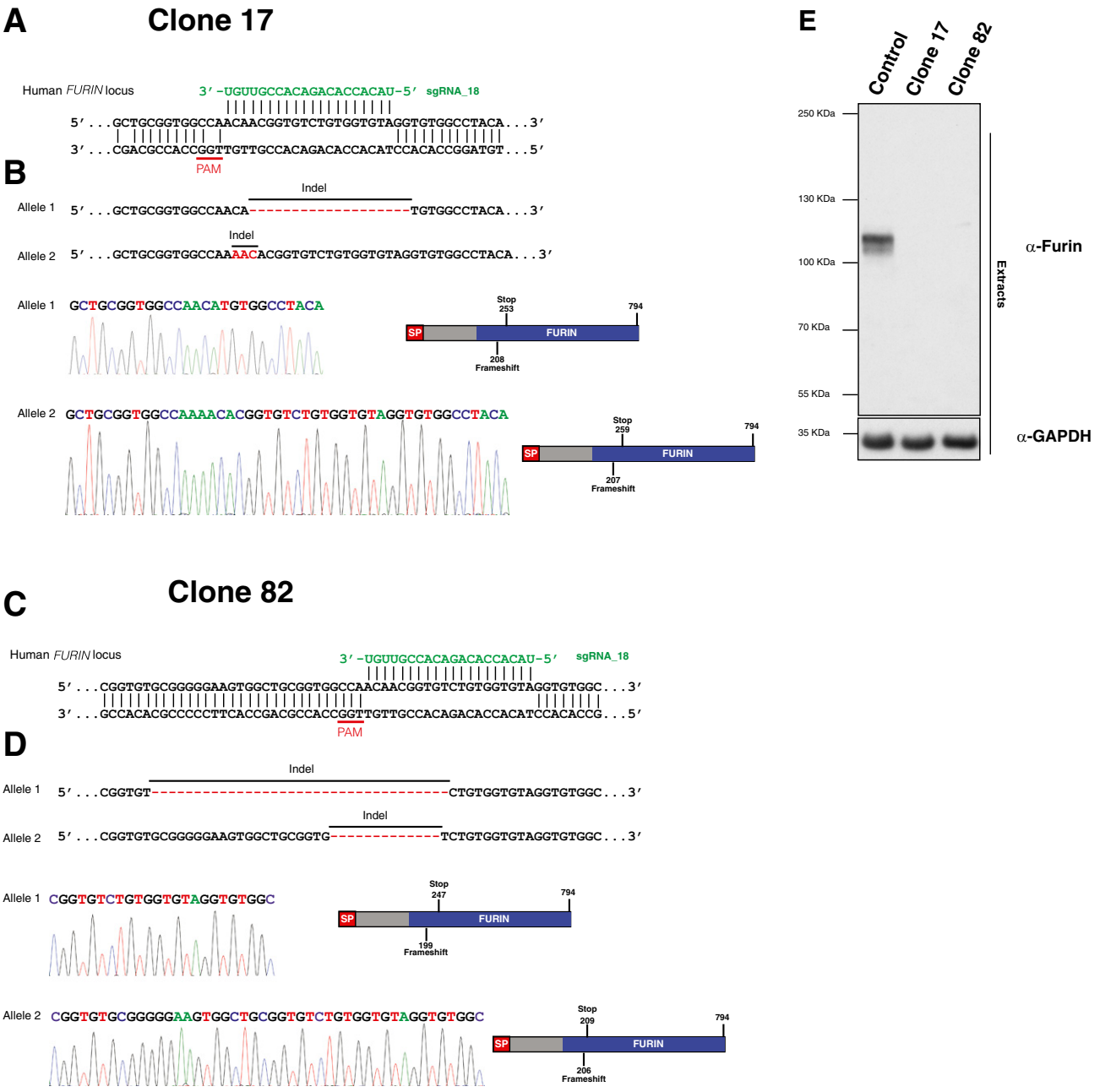

Fig. S7. Generation of *FURIN* knockout cells using CRISPR/Cas9 genome editing. (*A* and *C*) Schematic representations of the base pairing between a guide RNA (sgRNA_18) and the targeting locus of exon 7 in the human *FURIN* gene. (*B* and *D*) The sequences of the mutated alleles in *FURIN* clone 17 (*B*) and clone 82 (*D*) and representative chromatograms depicting the indels (red) are shown. The indels are predicted to cause frameshift mutations producing inactive copies of the protein. (*E*) Protein immunoblotting of cell extracts from control and furin KO cells.

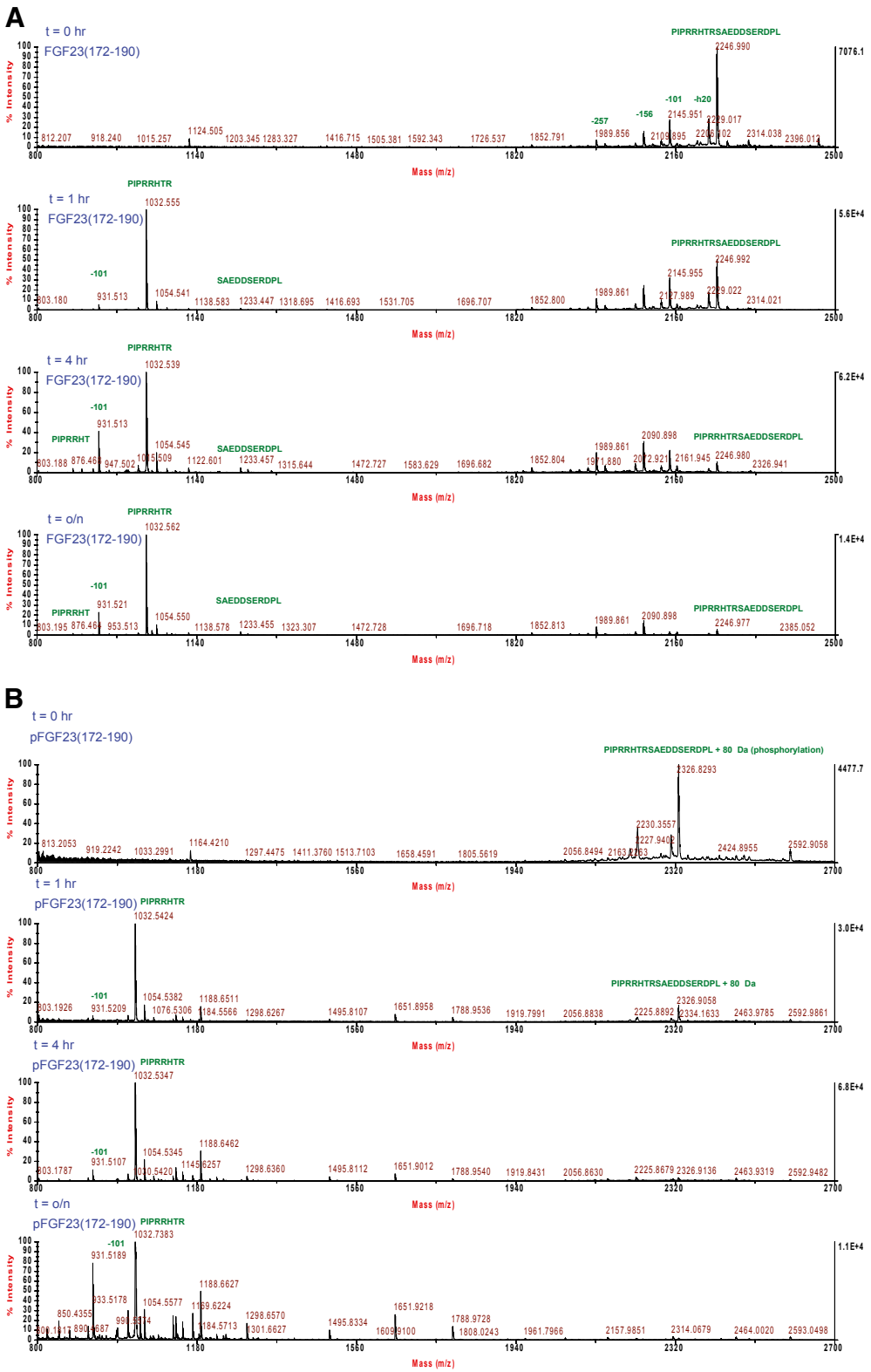

Fig. S8. Ser^{180}-phosphorylated FGF23(172–190) is cleaved by furin. Full MALDI-TOF MS spectra depicting the time-dependent cleavage of FGF23(172–190) (*A*) or Ser^{180}-phosphorylated FGF23(172–190) (*B*).

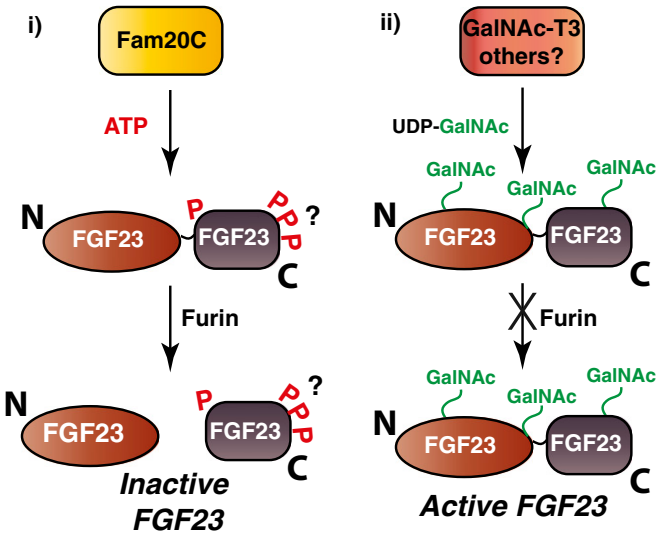

Fig. S9. Model for the regulation of FGF23 by Fam20C. We propose that interplay between phosphorylation by Fam20C (i) and O-glycosylation by GalNAc-T3 (ii) regulates the processing and activity of FGF23 by furin. Phosphorylation of FGF23 at Ser^{180} by Fam20C inhibits GalNAc-T3-mediated O-glycosylation at Thr^{178} and promotes inactivation by furin. Fam20C may also phosphorylate predicted Ser-x-Glu/pSer residues in the C-terminal region of FGF23.